Supplemental Material for

Interaction of Mechanical Oscillators

Mediated by the Exchange of Virtual Photon Pairs

I. DIAGONALIZATION OF THE STANDARD OPTOMECHANICS HAMILTONIAN

We consider a system constituted by two vibrating mirrors interacting via radiation pressure [see Fig. 1(a) in the main paper]. Both the cavity field and the displacements of the mirrors are treated as dynamical variables and a canonical quantization procedure is adopted [1, 2].

By considering only one mechanical mode for each mirror, with resonance frequency ω_i ($i = 1, 2$) and bosonic operators $\hat{b}_i$ and $\hat{b}_i^\dagger$, the displacement operators can be expressed as $\hat{x}_i = X_{\mathrm{zpf}}^{(i)}(\hat{b}_i^\dagger + \hat{b}_i)$, where $X_{\mathrm{zpf}}^{(i)}$ is the zero-point-fluctuation amplitude of the ith mirror. We also consider a single-mode optical resonator with frequency ω_{c} and bosonic photon operators $\hat{a}$ and $\hat{a}^\dagger$. The system Hamiltonian can be written as $\hat{H}_{\mathrm{s}} = \hat{H}_0 + \hat{H}_{\mathrm{I}}$, where

$$\hat{H}_0 = \omega_{\mathrm{c}}\hat{a}^\dagger\hat{a} + \omega_1\hat{b}_1^\dagger\hat{b}_1 + \omega_2\hat{b}_2^\dagger\hat{b}_2\,, \tag{S1}$$

is the unperturbed Hamiltonian. The Hamiltonian describing the mirror-field interaction is

$$\hat{H}_{\mathrm{I}} = (\hat{a} + \hat{a}^\dagger)^2 \sum_{i=1,2} \frac{g_i}{2}(\hat{b}_i + \hat{b}_i^\dagger)\,, \tag{S2}$$

where g_i are the coupling rates. Eq. (S2) is a direct generalization of the Law optomechanical Hamiltonian [1]. The linear dependence of the interaction Hamiltonian on the mirror operators is a consequence of the usual small-displacement assumption [1]. Once such linear dependence is assumed, the generalization (S2) to two mirrors, coupled to the same optical resonator, is straightforward. Equation (S2) has a clear physical meaning: the radiation pressure force acting on the mechanical resonators is proportional to the square modulus of the electric field.

By developing the photonic operators in normal order, and by defining new bosonic phonon and photon operators and a renormalized photon frequency, $\hat{H}_{\mathrm{s}}$ can be written as

$$\hat{H}_{\mathrm{s}} = \hat{H}_{\mathrm{om}} + \hat{V}_{\mathrm{DCE}}\,, \tag{S3}$$

where $\hat{V}_{\mathrm{DCE}}$ is the DCE interaction term:

$$\hat{V}_{\mathrm{DCE}} = (\hat{a}^2 + \hat{a}^{\dagger 2}) \sum_{i=1,2} \frac{g_i}{2} (\hat{b}_i + \hat{b}_i^\dagger), \tag{S4}$$

and $\hat{H}_{\mathrm{om}}$ is the standard optomechanics Hamiltonian:

$$\hat{H}_{\mathrm{om}} = \hat{H}_0 + \hat{V}_{\mathrm{om}} \tag{S5}$$

with

$$\hat{V}_{\mathrm{om}} = \hat{a}^\dagger \hat{a} \sum_{i=1,2} g_i (\hat{b}_i + \hat{b}_i^\dagger). \tag{S6}$$

$\hat{H}_{\mathrm{om}}$ can be easily diagonalized defining the displacement operators for the two mirrors. In particular, defining $(i = 1, 2)$

$$\hat{B}_i = \hat{b}_i + \beta_i \hat{a}^\dagger \hat{a} \tag{S7}$$

with $\beta_i = g_i/\omega_i$, we obtain

$$\hat{H}_{\mathrm{om}} = \omega_{\mathrm{c}} \left[1 - \left(\frac{\beta_1^2 \omega_1}{\omega_{\mathrm{c}}} + \frac{\beta_2^2 \omega_2}{\omega_{\mathrm{c}}} \right) \hat{a}^\dagger \hat{a} \right] \hat{a}^\dagger \hat{a} + \omega_1 \hat{B}_1^\dagger \hat{B}_1 + \omega_2 \hat{B}_2^\dagger \hat{B}_2. \tag{S8}$$

It is possible to separate the Hilbert space spanned by the Hamiltonian eigenvectors into subspaces with a definite number of photons n. The eigenstates of $\hat{H}_{\mathrm{om}}$ can be labelled by three indexes: the first two labelling the mechanical occupation numbers (phonons) of the two mirrors, dressed by the presence of n cavity photons while the third label describes the number n of cavity photons. We use the following notation

$$|\psi_{k,q,n}\rangle = |k_n\rangle \otimes |q_n\rangle \otimes |n\rangle_c \equiv |k, q, n\rangle. \tag{S9}$$

In particular, the photon occupation number n determines the nth cavity-photon subspace, while the first two kets ($|k_n\rangle$ and $|q_n\rangle$) are the displaced mechanical Fock states, respectively, for the first and second mirror. The action of the dressed phonon operators on the eigenstates satisfy the relations

$$\hat{B}_1 |k_n, q_n, n\rangle = \sqrt{k} |(k-1)_n, q_n, n\rangle, \qquad \hat{B}_2 |k_n, q_n, n\rangle = \sqrt{q} |k_n, (q-1)_n, n\rangle,$$
$$\hat{B}_1^\dagger |k_n, q_n, n\rangle = \sqrt{(k+1)} |(k+1)_n, q_n, n\rangle, \qquad \hat{B}_2^\dagger |k_n, q_n, n\rangle = \sqrt{(q+1)} |k_n, (q+1)_n, n\rangle. \tag{S10}$$

The explicit expression of the single displaced Fock state $|k_n\rangle_i$ for the ith mirror is (note that from Eq. (S7) and in the subspace with n cavity photons we have $\hat{B}_i^\dagger = \hat{b}_i^\dagger + n\beta_i\hat{I}_i$)

$$|k_n\rangle_i = \frac{1}{\sqrt{k!}}\hat{B}_i^{\dagger k}|0_n\rangle_i = \frac{1}{\sqrt{k!}}(\hat{b}_i^\dagger + n\beta_i\hat{I}_i)^k|0_n\rangle_i\,, \tag{S11}$$

where n-photons manifold and $|0_n\rangle_i$ is the coherent ground state for mirror i with n cavity photons, as is shown by the relation

$$\hat{b}_i|0_n\rangle_i = -n\beta_i|0_n\rangle_i\,, \tag{S12}$$

obtained using Eq. (S7) in $\hat{B}_i|0_n\rangle_i = 0$. Using the displacement operator $\hat{D}(n\beta_i) = \exp[n\beta_i(\hat{b}_i - \hat{b}_i^\dagger)]$, we have

$$|0_n\rangle_i = \hat{D}(n\beta_i)|0\rangle_i = \sum_j e^{-|n\beta_i|^2/2}\frac{(-n\beta_i)^j}{\sqrt{j!}}|j\rangle_i\,. \tag{S13}$$

In addition, from the relation $\hat{D}(n\beta)\hat{b}^\dagger\hat{D}^\dagger(n\beta) = b^\dagger + n\beta$ [3], using Eqs. (S11) and (S13), we obtain

$$|k_n\rangle_i = \frac{1}{\sqrt{k!}}(\hat{b}_i^\dagger + n\beta_i\hat{I}_i)^k|0_n\rangle_i = \frac{1}{\sqrt{k!}}(\hat{b}_i^\dagger + n\beta_i\hat{I}_i)^k\hat{D}(n\beta_i)|0\rangle = \hat{D}(n\beta_i)\frac{1}{\sqrt{k!}}\hat{b}_i^{\dagger k}|0\rangle = \hat{D}(n\beta_i)|k_0\rangle \tag{S14}$$

Finally, after a little bit of algebra, we have

$${}_i\langle k_0'|k_n\rangle_i = {}_i\langle k_0'|[\hat{D}(n\beta_i)]|k_0\rangle_i = D_{k',k}(n\beta_i) = \sqrt{k!/k'!}(n\beta_i)^{k'-k}e^{-|n\beta_i|^2/2}L_k^{k'-k}(|n\beta_i|^2)\,, \tag{S15}$$

where $L_k^p(x)$ are the associated Laguerre polynomials.

In conclusion, the standard optomecanical Hamiltonian can be diagonalized as shown above and we obtain

$$\hat{H}|k,q,n\rangle = E_{k,q,n}|k,q,n\rangle\,, \tag{S16}$$

where

$$E_{k,q,n} = \omega_c n\left[1 - \left(\frac{\beta_1^2\omega_1}{\omega_c} + \frac{\beta_2^2\omega_2}{\omega_c}\right)n\right] + \omega_1 k + \omega_2 q\,, \tag{S17}$$

or, in more compact form [replacing for clarity the phonon labels as $(k,q) \to (k_1,k_2)$]

$$E_{k_1,k_2,n} = \omega_c n - \sum_i g_i^2 n^2/\omega_i + \sum_i \omega_i k_i\,. \tag{S18}$$

II.   THE DCE INTERACTION HAMILTONIAN AS A PERTURBATION

In this section, we introduce the DCE interaction term. We consider this additional contribution as a perturbation to the optomechanical Hamiltonian $\hat{H}_{\rm om}$. This additional term creates and destroys photon pairs. Here we consider processes at the lowest nonzero perturbation order. Thus we limit our calculations to the subspace containing zero and two cavity photons. The DCE interaction Hamiltonian $\hat{V}_{\rm DCE}$ is calculated using second-order perturbation theory. These perturbative calculations are carried out using the James' method [4]:

$$\hat{H}_{\rm eff}^{(2)} = \frac{1}{i}\hat{V}_{\rm DCE}^{I(0,2)}(t)\int_0^t \hat{V}_{\rm DCE}^{I(0,2)}(t')dt'\,, \tag{S19}$$

where

$$\hat{V}_{\rm DCE}^{I(0,2)}(t) = e^{i\hat{H}t}\hat{V}_{\rm DCE}^{(0,2)}e^{-i\hat{H}t}$$

is the projection operator $\hat{V}_{\rm DCE}$ acting in the subspace containing 0 and 2 photons expressed in the interaction picture. After some algebra, we obtain (we assume $g_1 = g_2 \equiv g$):

$$\hat{V}_{\rm DCE}^{I(0,2)}(t) = \frac{g}{2}\sum_{\substack{k\ q\\k'\ q'}} A_{k\ q}^{k'\ q'}\,|k_2,q_2,2\rangle\langle k_0',q_0',0|\,e^{i\omega_{k\ q}^{k'\ q'}t} + (A_{k\ q}^{k'\ q'})^\dagger\,|k_0',q_0',0\rangle\langle k_2,q_2,2|\,e^{-i\omega_{k\ q}^{k'\ q'}t} \tag{S20}$$

where

$$\omega_{k\ q}^{k'\ q'} = 2\Omega_{\rm c} + (k'-k)\omega_1 + (q'-q)\omega_2; \tag{S21}$$

with $\Omega_{\rm c} = 1 + \tilde{\beta}_1 + \tilde{\beta}_2$, $\tilde{\beta}_i = g^2/(\omega_i\omega_{\rm c})$. We also have:

$$A_{k\ q}^{k'\ q'} = \left\langle k_2,q_2,2\left|\hat{V}_{\rm DCE}\right|k_0',q_0',0\right\rangle\,;$$

that can be expressed in more explicit form as

$$A_{k\ q}^{k'\ q'} = \sqrt{2}\left\{[\sqrt{k'}\langle k_2|(k'-1)_0\rangle + \sqrt{k'+1}\langle k_2|(k'+1)_0\rangle]\langle q_2|q_0'\rangle +\right.$$
$$\left.[\sqrt{q'}\langle q_2|(q'-1)_0\rangle + \sqrt{q'+1}\langle q_2|(q'+1)_0\rangle]\langle k_2|k_0'\rangle\right\}\,. \tag{S22}$$

Note that $A_{k\ q}^{k'\ q'} = A_{k'\ q'}^{\dagger k\ q}$. Using $D_{k',k}(2\beta_i) = \langle k_2'|k_0\rangle$, we have:

$$A_{k\ q}^{k'\ q'} = \sqrt{2}[\sqrt{k'}D_{k,k'-1}(2\beta_1) + \sqrt{k'+1}D_{k,k'+1}(2\beta_1)]D_{q,q'}(2\beta_2) +$$
$$\sqrt{2}[\sqrt{q'}D_{q,q'-1}(2\beta_2) + \sqrt{q'+1}D_{q,q'+1}(2\beta_2)]D_{k,k'}(2\beta_1)\,, \tag{S23}$$

where the matrix elements of the displacement operators can be expressed in terms of associated Laguerre polynomials: $D_{k',k}(\alpha) = \sqrt{k!/k'!}\alpha^{k'-k}e^{-|\alpha|^2/2}L_k^{k'-k}(|\alpha|^2)$.

4

A. One phonon – zero photons subspace

The $(1+0)$ subspace containing zero photons and one phonon excitation is spanned by the eigenvectors $|1, 0, 0\rangle$ and $|0, 1, 0\rangle$. At $\omega_2 \sim \omega_1$, these states are degenerate in absence of the $\hat{V}_{\mathrm{DCE}}$ interaction. In presence of such interaction, degeneracy is removed and an avoided level crossing can be observed. This effect can be described by introducing an effective Hamiltonian. Specifically: a) we introduce Eq. (S20) into Eq. (S19); b) we perform the integration; c) we limit the calculations to matrix elements containing zero photons; d) we transform back to the Schrödinger picture; e) finally, we project the result into the $(1+0)$ subspace spanned by the vectors $|1, 0, 0\rangle$, $|0, 1, 0\rangle$. We obtain

$$\hat{H}_{\mathrm{eff}} = \hat{H}_{\mathrm{eff}}^0 + [\lambda_{01}^{10} |0, 1, 0\rangle\langle 1, 0, 0| + \mathrm{H.c.}], \tag{S24}$$

where

$$\hat{H}_{\mathrm{eff}}^0 = \Omega_1 |1, 0, 0\rangle\langle 1, 0, 0| + \Omega_2 |0, 1, 0\rangle\langle 0, 1, 0|, \tag{S25}$$

with $\Omega_1 = \omega_1 + \Delta_{10}$ and $\Omega_2 = \omega_2 + \Delta_{01}$, and with

$$\Delta_{10} = -\frac{g^2}{4} \sum_{kq} \frac{A_{kq}^{10\dagger} A_{kq}^{10}}{2\Omega_{\mathrm{c}} + (k-1)\omega_1 + q\omega_2}; \tag{S26}$$

$$\Delta_{01} = -\frac{g^2}{4} \sum_{kq} \frac{A_{kq}^{01\dagger} A_{kq}^{01}}{2\Omega_{\mathrm{c}} + k\omega_1 + (q-1)\omega_2}; \tag{S27}$$

$$\lambda_{01}^{10} = -\frac{g^2}{4} \sum_{kq} \frac{A_{kq}^{01\dagger} A_{kq}^{10}}{2\Omega_{\mathrm{c}} + (k-1)\omega_1 + q\omega_2}. \tag{S28}$$

In Fig. S1, we show a comparison between the numerically calculated normalized Rabi splitting $(2\lambda_{01}^{10}\omega_1)$ between the two one-phonon states $|1, 0, 0\rangle$ and $|0, 1, 0\rangle$ and the corresponding theoretical value calculated using second-order perturbation theory as a function of the normalized optomechanical coupling g/ω_1. The agreement is very good for g/ω_1 below 0.1.
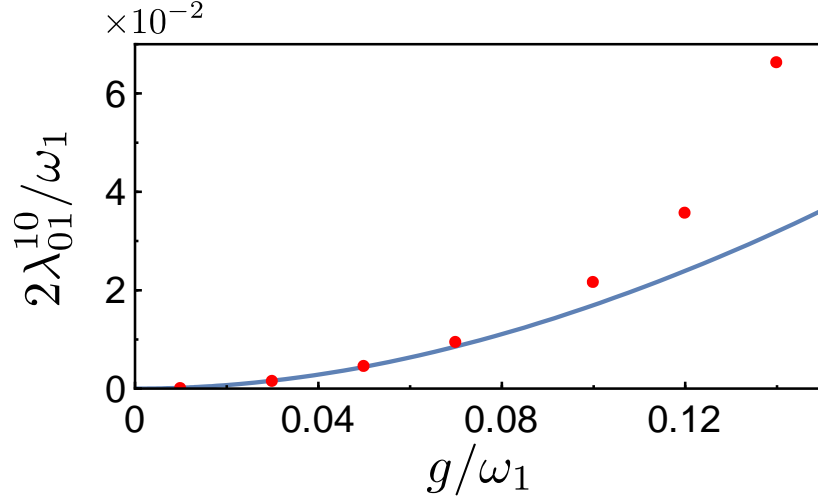
Figure S1. Comparison between the numerically calculated normalized Rabi splitting (red points) (corresponding to twice the effective coupling between the two one-phonon states $|1, 0, 0\rangle$ and $|0, 1, 0\rangle$) and the corresponding calculation using second-order perturbation theory (solid blue curve).

B. Two phonons – zero photons subspace

The $(2 + 0)$ subspace with zero photons in the cavity and containing two phonon excitations is spanned by the eigenvectors: $|2, 0, 0\rangle$, $|0, 2, 0\rangle$ and $|1, 1, 0\rangle$. Also in this case, at $\omega_2 \sim \omega_1$, these states are degenerate in the absence of the $\hat{V}_{\mathrm{DCE}}$ interaction. With the introduction of $\hat{V}_{\mathrm{DCE}}$, degeneracy is removed, and an avoided level crossing can be observed. Following the same procedure described in the previous subsection, this effect can be described by introducing an effective Hamiltonian acting on the $(2 + 0)$ subspace. We obtain:

$$\hat{H}_{\mathrm{eff}} = \hat{H}_{\mathrm{eff}}^0 + [\lambda_{20}^{02} |2, 0, 0\rangle\langle 0, 2, 0| + \lambda_{20}^{11} |2, 0, 0\rangle\langle 1, 1, 0| + +\lambda_{02}^{11} |0, 2, 0\rangle\langle 1, 1, 0| + \mathrm{H.c.}]; \quad \text{(S29)}$$

where

$$\hat{H}_{\mathrm{eff}}^0 = \Omega_{20} |0, 2, 0\rangle\langle 0, 2, 0| + \Omega_{02} |2, 0, 0\rangle\langle 2, 0, 0| + \Omega_{11} |1, 1, 0\rangle\langle 1, 1, 0|; \quad \text{(S30)}$$

with $\Omega_{20} = 2\omega_1 + \Delta_{20}$, $\Omega_{11} = \omega_1 + \omega_2 + \Delta_{11}$ and $\Omega_{02} = 2\omega_2 + \Delta_{02}$, and

$$\lambda_{20}^{02} = -\frac{g^2}{4} \sum_{kq} \frac{A_{kq}^{02\dagger} A_{kq}^{20}}{2\Omega_{\mathrm{c}} + (k - 2)\omega_1 + q\omega_2}, \quad \text{(S31)}$$

6

$$\lambda_{20}^{11} = -\frac{g^2}{4} \sum_{kq} \frac{A_{kq}^{11\dagger} A_{kq}^{20}}{2\Omega_{\mathrm{c}} + (k-2)\omega_1 + q\omega_2}, \tag{S32}$$

$$\lambda_{02}^{11} = -\frac{g^2}{4} \sum_{kq} \frac{A_{kq}^{11\dagger} A_{kq}^{02}}{2\Omega_{\mathrm{c}} + k\omega_1 + (q-2)\omega_2}, \tag{S33}$$

$$\Delta_{20} = -\frac{g^2}{4} \sum_{kq} \frac{A_{kq}^{20\dagger} A_{kq}^{20}}{2\Omega_{\mathrm{c}} + (k-2)\omega_1 + q\omega_2}, \tag{S34}$$

$$\Delta_{02} = -\frac{g^2}{4} \sum_{kq} \frac{A_{kq}^{02\dagger} A_{kq}^{02}}{2\Omega_{\mathrm{c}} + k\omega_1 + (q-2)\omega_2}, \tag{S35}$$

$$\Delta_{11} = -\frac{g^2}{4} \sum_{kq} \frac{A_{kq}^{11\dagger} A_{kq}^{11}}{2\Omega_{\mathrm{c}} + (k-1)\omega_1 + (q-1)\omega_2}. \tag{S36}$$

A comparison of these perturbative analytical results with the numerical result is provided in the Tables I and II. The discrepancies can be ascribed to higher-order terms that at a coupling strength $g/\omega_1 = 0.1$ provide non-negligible contributions.

	$2\lambda_{01}^{10}$	$2\lambda_{20}^{11}$	$2\lambda_{20}^{02}$	$2\lambda_{02}^{11}$
Numerical $\simeq$	0.0217	0.0217	0.0384	0.0167
Theoretical $\simeq$	0.0170	0.0171	0.0348	0.0177

Table I. Comparison between the effective splittings calculated both numerically (as difference between the eigenvalues) and analytically using the James' method [4]. In particular, the theoretical values corresponding to $2\lambda_{20}^{11}$, $2\lambda_{20}^{02}$ and $2\lambda_{02}^{11}$ are obtained by the diagonalization of a 3×3 matrix representing the effective Hamiltonian in the subspace with two phonon excitations and zero photons. The cavity-mode resonance frequency is $\omega_{\mathrm{c}} = 0.85\,\omega_1$ and $\omega_2 = \omega_1$.

	Δ_{10}	Δ_{01}	Δ_{11}	Δ_{02}	Δ_{20}
Numerical $\simeq$	-0.0131	-0.0159	-0.0221	-0.0239	-0.0217
Theoretical $\simeq$	-0.0120	-0.0121	-0.0207	-0.0199	-0.0207

Table II. Comparison between the numerically calculated energy shifts and the analytical calculations obtained using the James' method. The mechanical frequency of mirror 2 is $\omega_2 = 0.94\,\omega_1$. For this value the energy levels investigated do not interact significantly, and hence the energy shifts are not affected by the level-repulsion effect that occurs when the mirrors are on resonance with each other. The cavity-mode resonance frequency is $\omega_c = 0.85\,\omega_1$.

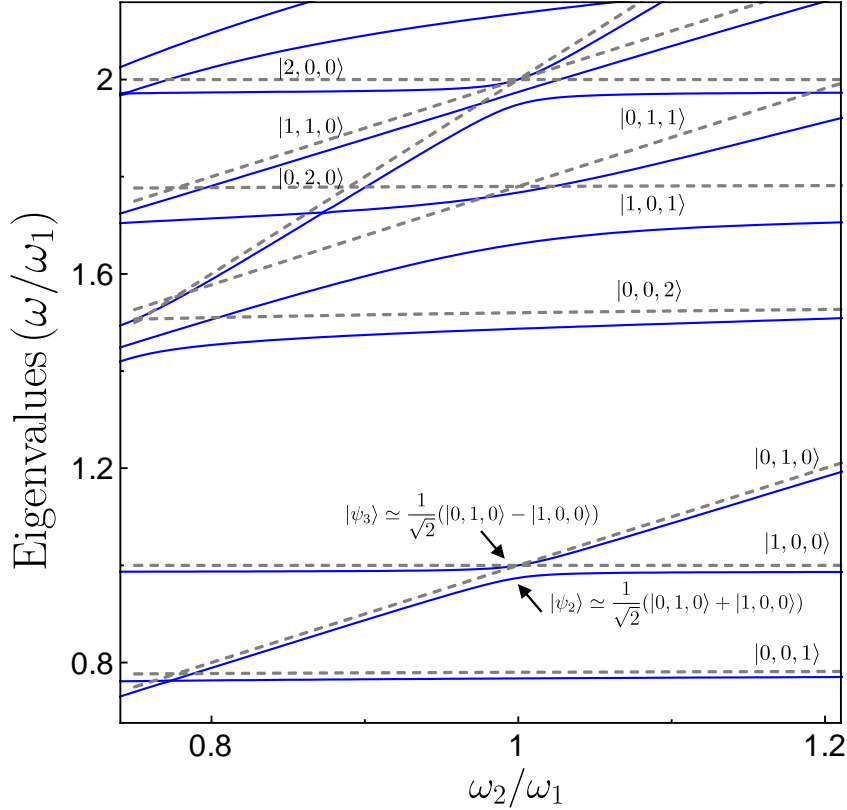## III. ENERGY LEVELS AND SPLITTINGS FOR DIFFERENT OPTOMECHANICAL COUPLINGS.

Figure S2. Lowest energy levels of the system Hamiltonian as a function of ω_2/ω_1. We used $g/\omega_1 = 0.1$ and $\omega_c/\omega_1 = 0.8$.
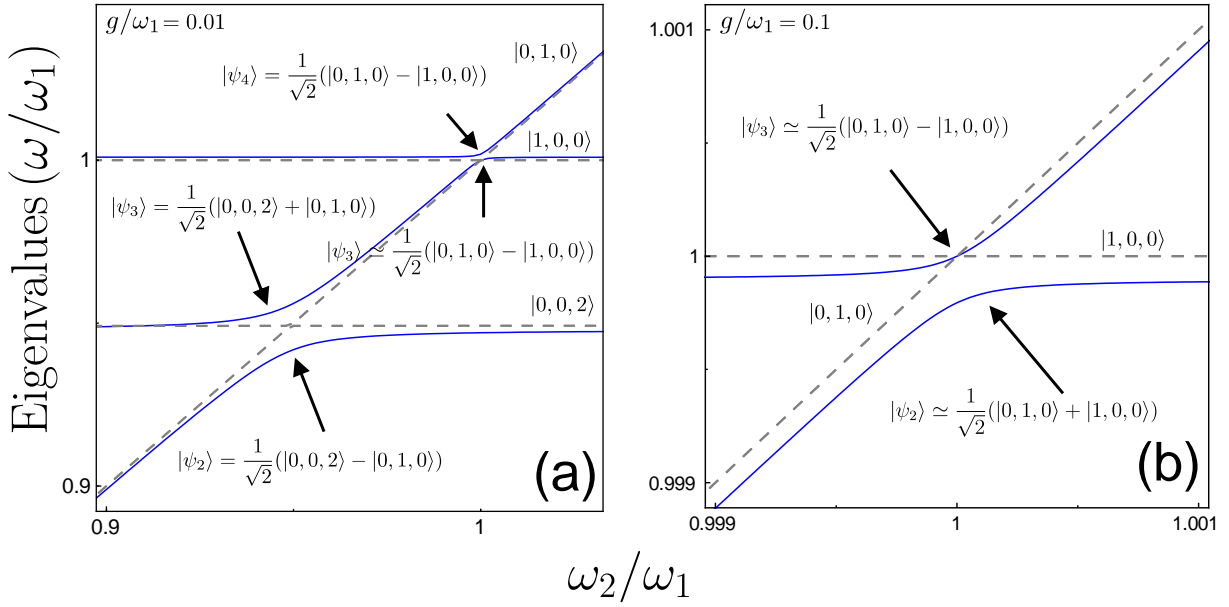
Figure S3. Relevant lowest energy levels of the system Hamiltonian as a function of ω_2/ω_1. Panel (a) has been obtained using $g/\omega_1 = 0.01$ and $\omega_c/\omega_1 = 0.475$. Panel (b) has been obtained with the same parameters of Fig. S2.

Figure S2 displays the lowest energy levels $E_j - E_0$ of the system Hamiltonian as a function of the ratio between the mechanical frequency of mirror 2 and that of mirror 1. An optome-chanical coupling $g/\omega_1 = 0.1$ has been used, the cavity-mode resonance frequency is $\omega_c = 0.8\,\omega_1$. Starting from the lowest energy levels, we first avoided level crossing originates from the coherent coupling of the zero-photon states $|1,0,0\rangle$ and $|0,1,0\rangle$. At the minimum energy splitting, the resulting states are well approximated by $|\psi_{2,3}\rangle \simeq (1/\sqrt{2})(|1,0,0\rangle \pm |0,1,0\rangle)$. As shown in the main paper and in the previous section, this mirror-mirror interaction is a result of virtual exchange of cavity photon pairs. This coherent coupling is greatly enhanced by the presence of a cavity photon, resulting in the larger splitting $(E_6 - E_5)$, corresponding to the states $|\psi_{5,6}\rangle \simeq (1/\sqrt{2})(|1,0,1\rangle \pm |0,1,1\rangle)$. At higher energy, at $\omega_2/\omega_1 \sim 1$, $\hat{V}_{\mathrm{DCE}}$ removes the degeneracy between the three states $|2,0,0\rangle$, $|0,2,0\rangle$, and $|1,1,0\rangle$, determining a two-phonon coupling between the two mirrors.

Figure S3 shows the relevant energy levels of the system Hamiltonian $\hat{H}_s$ as a function of the ratio ω_2/ω_1. For the panel (a) an optomechanical coupling $g/\omega_1 = 0.01$ has been used and the cavity-mode resonance frequency is $\omega_c = 0.475\,\omega_1$. The lowest energy anticrossing corresponds to the resonance condition for the DCE. The higher energy one is the signature

9

of the mirror-mirror interaction mediated by the virtual DCE photons. At the minimum energy splitting $2\lambda_{10}^{01} \simeq 1,85 \times 10^{-2}\omega_1$, the resulting states are well approximated by $|\psi_{3,4}\rangle \simeq (1/\sqrt{2})(|1,0,0\rangle \pm |0,1,0\rangle)$. In panel (b) we use $g/\omega_1 = 0.1$. In this case the cavity-mode resonance frequency is $\omega_c = 0.8\,\omega_1$. Also in this case, the anticrossing is the signature of the mirror-mirror interaction mediated by the virtual DCE photons. At the minimum energy splitting $2\lambda_{10}^{01} \simeq 2,56 \times 10^{-2}\omega_1$, the resulting states are well approximated by $|\psi_{2,3}\rangle \simeq (1/\sqrt{2})(|1,0,0\rangle \pm |0,1,0\rangle)$.

IV. SYSTEM DYNAMICS UNDER A SINGLE-TONE CONTINUOUS-WAVE MECHANICAL DRIVE: ADDITIONAL RESULTS

We start investigating the system dynamics at $T = 0$, with the system starting from its ground state, and introducing the excitation of mirror 1 by a single-tone continuous-wave mechanical drive $\mathcal{F}_1(t) = \mathcal{A}\cos\left(\omega_d t\right)$, with $\omega_d = \omega_1$. Figure S4 shows the time evolution of the mean phonon numbers of the two mirrors $\langle \hat{B}_i^\dagger \hat{B}_i \rangle$ and of the intracavity mean photon number $\langle \hat{A}^\dagger \hat{A} \rangle$. Here $\hat{A}, \hat{B}_i$ are the *physical* photon and phonon operators (see main paper). We assume a zero-temperature reservoir and use $\gamma_1 = \gamma_2 = \gamma = \omega_1/260$ and $\kappa = \gamma$ for the mechanical and photonic loss rates. We consider a weak ($\mathcal{A}/\gamma = 0.95$) resonant excitation of mirror 1. Panel (a) has been obtained using $g/\omega_1 = 0.1$ and $\omega_c/\omega_1 = 0.8$. Panel (b) using $g/\omega_1 = 0.03$ and $\omega_c/\omega_1 = 0.495$. Panel (c) using $g/\omega_1 = 0.01$ and $\omega_c/\omega_1 = 0.475$. We set $\omega_2 = \omega_1$. The results shown in Fig. S4 demonstrate that the excitation transfer mechanism via virtual DCE photon pairs, proposed here, works properly. In steady state, mirror 2 reaches almost the same excitation intensity as the driven mirror 1 at normalized couplings $g = 0.1$ and $g = 0.03$. The photon population remains very low throughout the considered time window. In Fig. S5, in order to obtain the maximum excitation transfer between the two mirrors (despite the small coupling strength $g/\omega_1 = 0.01$), we investigate the system dynamics using $\omega_c = 0.5\,\omega_1$. We also consider the system initially in a thermal state with a normalized thermal energy $kT/\omega_1 = 0.208$, corresponding to a temperature $T = 60$ mK for $\omega_1/2\pi = 6$ GHz. During, its time evolution, the system interacts with thermal baths with the same temperature T. The obtained results show that a good mechanical transfer is achieved. However, in this case, a significant amount of real photon pairs are generated. This configuration can be used to probe the DCE effect in the presence of thermal photons.
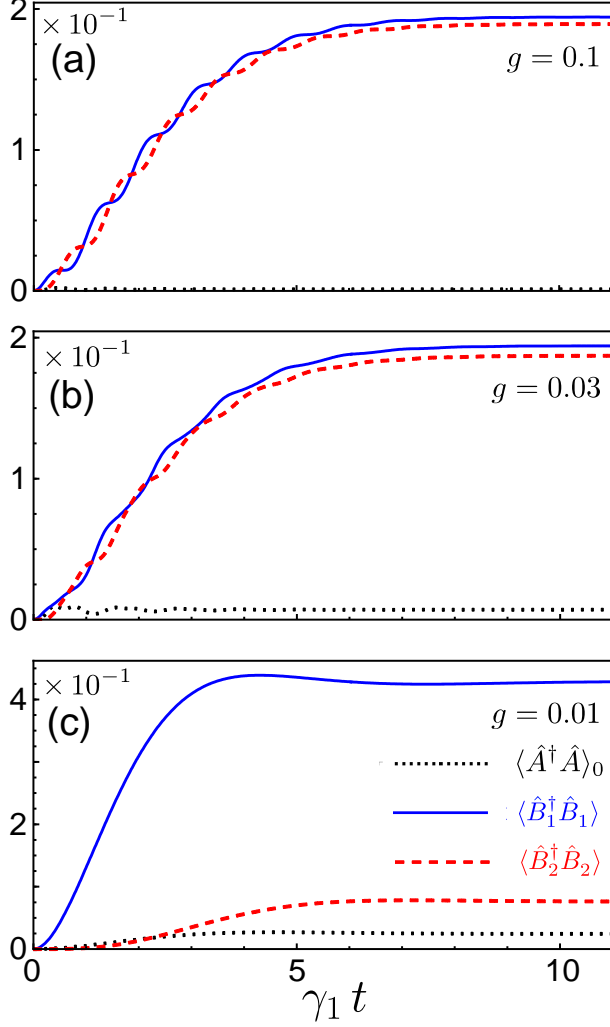
Figure S4. System dynamics under continuous-wave drive of mirror 1 for different optomechanical coupling strengths. The blue solid and red dashed curves describe the mean phonon numbers $\langle \hat{B}_1^\dagger \hat{B}_1 \rangle$ and $\langle \hat{B}_2^\dagger \hat{B}_2 \rangle$, respectively, while the black dotted curve describes the mean intracavity photon number $\langle \hat{A}^\dagger \hat{A} \rangle$. Parameters are given in the text.

V. MECHANICAL EXCITATION TRANSFER: PULSED EXCITATION

We now investigate the transfer of mechanical excitations mediated by virtual photon pairs by exciting mirror 1 with a resonant Gaussian pulse:

$$\mathcal{F}_1(t) = \mathcal{A}\,\mathcal{G}(t - t_0)\cos{(\omega_{\mathrm{d}}\,t)},$$

where $\omega_{\mathrm{d}} = \omega_1$, and $\mathcal{G}(t)$ is a normalized Gaussian function with standard deviation $\sigma = 1/(10\lambda_{10}^{01})$. We consider the case of the strong coupling regime, when the mirror-mirror
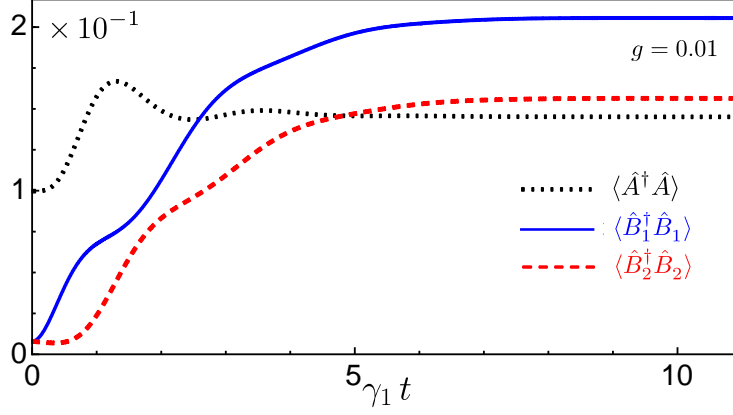
11

Figure S5. System dynamics for $\omega_c = 0.5\omega_1$ under continuous-wave drive of mirror 1, normalized coupling $g/\omega_1 = 0.01$ and T= 60 mK. The blue solid and red dashed curves describe the mean phonon numbers $\langle \hat{B}_1^\dagger \hat{B}_1 \rangle$ and $\langle \hat{B}_2^\dagger \hat{B}_2 \rangle$, respectively, while the black dotted curve describes the mean intracavity photon number $\langle \hat{A}^\dagger \hat{A} \rangle$ arising due to the DCE.
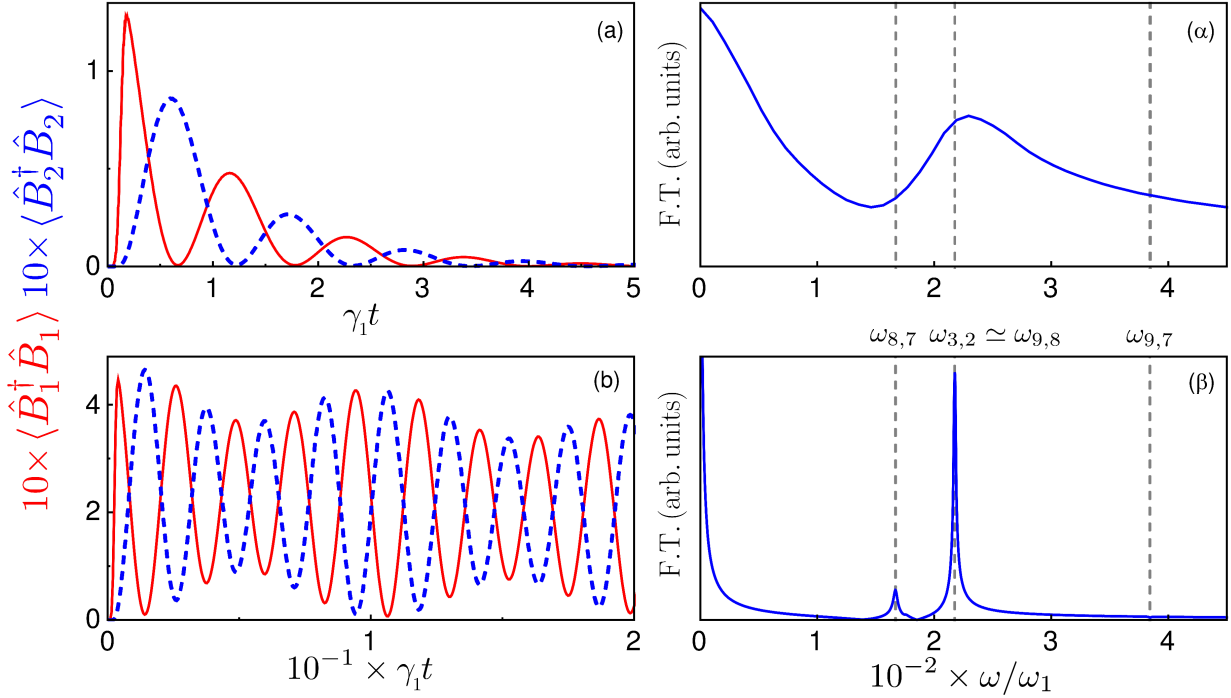

Figure S6. Time evolution of the mean phonon numbers of the two mirrors after the arrival of the pulse. We consider two different amplitudes which increase from top to bottom: $\mathcal{A} = 0.25\,\pi$ (a), 0.45π (b). Specifically, panels (a-b) display the mean phonon numbers $\langle \hat{B}_i^\dagger \hat{B}_i \rangle$. Panels ($\alpha$-$\beta$) display the Fourier transform of the mean phonon number shown in the corresponding panel on the left. Other parameters are given in the text.

12

coupling strength λ_{10}^{01} is larger than the total decoherence rate $\gamma_1 + \gamma_2$. We set the resonance frequency of mirror 2 to $\omega_2 \simeq \omega_1$ providing the minimum level splitting $2\lambda_{10}^{01}$. The system starts in its ground state. Figure S6 displays the system dynamics after the pulse arrival and the Fourier transform of the mean phonon number of mirror 1 (no relevant changes occur for mirror 2), obtained for pulses with amplitudes increasing from top to bottom: $\mathcal{A} = 0.25\pi, 0.45\pi$. Panels S6(a) and S6($\alpha$) have been obtained using the loss rates $\gamma = 3.5 \times 10^{-3}\omega_1$ and $\kappa = 0.5\gamma$. Figure S6(a) displays coherent and reversible sinusoidal oscillations (with peak amplitudes decaying exponentially), showing that the mechanical state of the spatially separated mirrors is transferred from one to the other at a rate $\omega_{3,2} \equiv E_3 - E_2 = \lambda_{10}^{01}$, as confirmed by the peak in the Fourier transform in Fig. S6(α). We notice that the position and broadening of the peak at $\omega_{3,2}$ in Fig. S6(α) is influenced by the initial dynamics of $\langle \hat{B}_1^\dagger \hat{B}_1 \rangle$, which in turn is affected by the pulse shape (Fig. S7 displays the corresponding spectrum for mirror 2). The higher peak at $\omega = 0$ originates from the exponential decay of the signal. These results clearly show that, for the weaker excitation amplitude ($\mathcal{A} = 0.25\pi$), only the one-phonon states $|1, 0, 0\rangle$ and $|0, 1, 0\rangle$ are excited significantly and contribute to the dynamics.
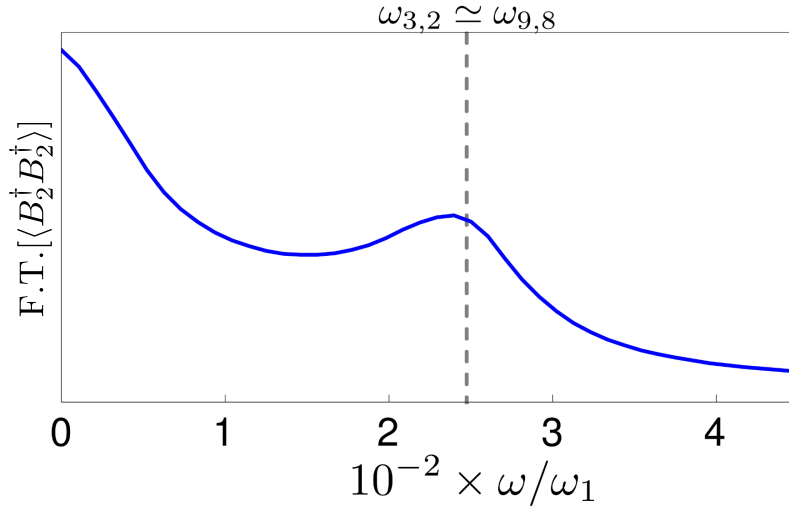

Figure S7.   Fourier transform of the mean phonon number of mirror 2 obtained for a pulse with amplitude $\mathcal{A} = 0.25\pi$.

By increasing the pulse amplitude [Fig. S6(b)], the mean phonon numbers grow significantly and the signals are no more sinusoidal, owing to the additional excitation of the states $|2, 0, 0\rangle$, $|1, 1, 0\rangle$, and $|0, 2, 0\rangle$, whose DCE-induced coupling gives rise to the hybridized

energy eigenstates $|\psi_7\rangle$, $|\psi_8\rangle$, and $|\psi_9\rangle$. In order to better distinguish the nonsinusoidal behaviour, we used much lower loss rates: $\gamma = 8 \times 10^{-5}\omega$ and $\kappa = 0.5\gamma$. Figure S6(β) shows the appearence of an additional peak at $\omega = \omega_{8,7}$, confirming that higher-energy mechanical states get excited. We observe that the frequency splitting $\omega_{9,8}$ is very close to $\omega_{3,2}$, hence, it does not give rise to a new peak in Fig. S6(β). Moreover, the frequency splitting at $\omega_{9,7}$ does not contribute significantly to the dynamics as confirmed by the spectrum in Fig. S6(β). An analytic calculation based on three coupled levels confirms that the used parameters give rise to a negligible contribution at $\omega_{9,7}$.

VI. MECHANICAL EXCITATION TRANSFER: NONADIABATIC EFFECTIVE SWITCHING OF THE INTERACTION

As pointed out in the last paragraph of the main paper, if it is possible to control the interaction time (as currently realized in superconducting artificial atoms), e.g., by rapidly changing the resonance frequencies of the mechanical oscillators, the interaction scheme proposed here would represent an attractive architecture for quantum information processing with optomechanical systems. Here we provide some examples of quantum state transfer. In Fig. S8, we show the phonon population dynamics obtained preparing the system in three different initial states (a) $|1, 0, 0\rangle$, (b) $\frac{1}{\sqrt{2}}(|0, 0, 0\rangle + |1, 0, 0\rangle)$, (c) $|2, 0, 0\rangle$. Mirror 2 is initially set at a mechanical frequency ω_2^{in}. This value must be chosen sufficiently far from the value $\omega_2^{\mathrm{min}} \simeq 0.99\,\omega_1$ corresponding to the minimum splitting between states $|1, 0, 0\rangle$ and $|0, 1, 0\rangle$. In particular, we have fixed $\omega_2^{\mathrm{in}} = \omega_2^{\mathrm{min}} - \delta$ with $\delta = 0.069\,\omega_1$. This value is also sufficiently far from the region where the avoided three-level crossing between the states $|\psi_i\rangle$ with $i = 7, 8, 9$ appears. Subsequently, a time-dependent perturbation $H_{\mathrm{na}} = f(t)\hat{B}_2^\dagger \hat{B}_2$ [with $f(t) \approx \theta(t - t_0)$] is introduced in order to modify the resonance frequency of mirror 2 (θ is the Heaviside step function). More specifically $f(t) = \delta\left[\sin^2[\Omega(t - t_0)\theta(t - t_0) + \sin^2[\Omega(t - t_f)\theta(t - t_f)]\right]$ is a smoothed step function, where δ fixes the change in mechanical frequency of mirror 2, t_0 is the time when the frequency starts to change, $t_f = t_0 + \pi/(2A)$, and Ω is the frequency setting the smoothness.

This enables a non-adiabatic transition from the frequency region with $\omega_2 = \omega_2^{\mathrm{in}}$, where the states $|2, 0, 0\rangle$, $|1, 0, 0\rangle$ and $|0, 1, 0\rangle$ are eigenstates of the system, to the frequency region $\omega_2 = \omega_2^{\mathrm{min}}$ where the former states are no longer eigenstates of the system. As a consequence,
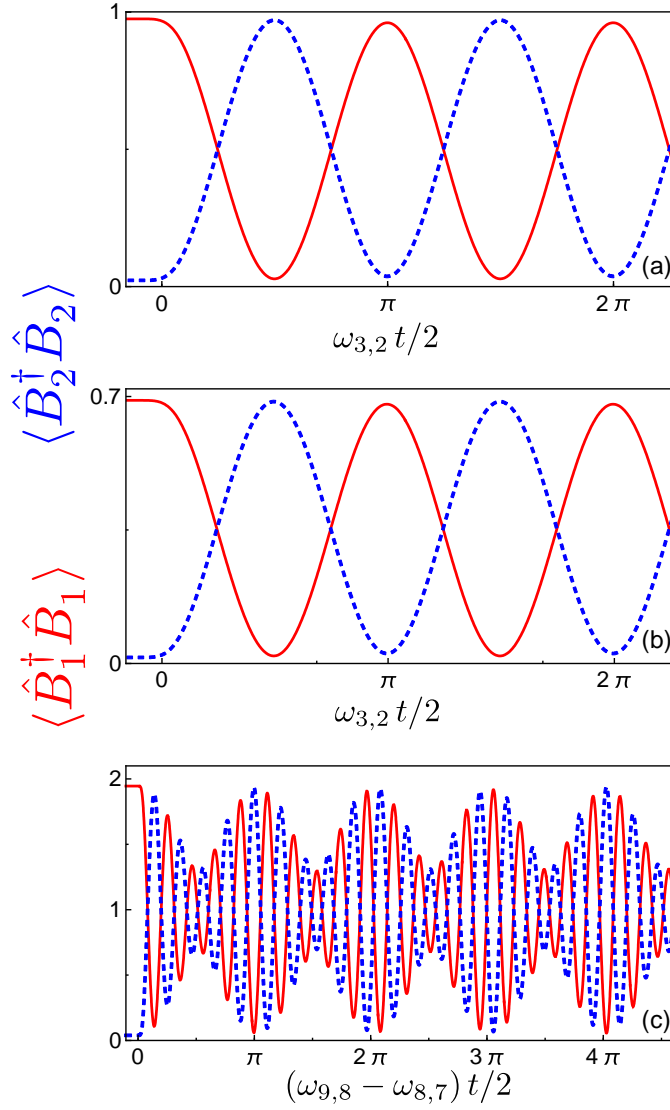
Figure S8. Time evolution of the mean phonon numbers of the two mirrors obtained preparing the system in an initial state (a) $|1, 0, 0\rangle$, (b) $\frac{1}{\sqrt{2}}(|1, 0, 0\rangle + |0, 0, 1\rangle)$, (c) $|2, 0, 0\rangle$. Mirror 2 is initially set at a mechanical frequency ω_2^{in} (details are given in the text). We note that the dynamics display oscillations, (a) and (b), due to the avoided level crossing between the states $|\psi_3\rangle$ and $|\psi_2\rangle$ with frequency equal to $\omega_{3,2}$; (c) due to the splittings between the states $|\psi_9\rangle$, $|\psi_8\rangle$ and $|\psi_7\rangle$, whose transitions from higher to lower levels give rise to beats (the details are given in the text).

the dynamics of the phonon populations of the two mirrors display *quantum Rabi-like* oscillations [see Fig. S8(a) and (b)] due to the avoided level crossing between the states $|\psi_3\rangle$ and $|\psi_2\rangle$ (the eigenstates of the systems are, in this frequency region, the symmetric and
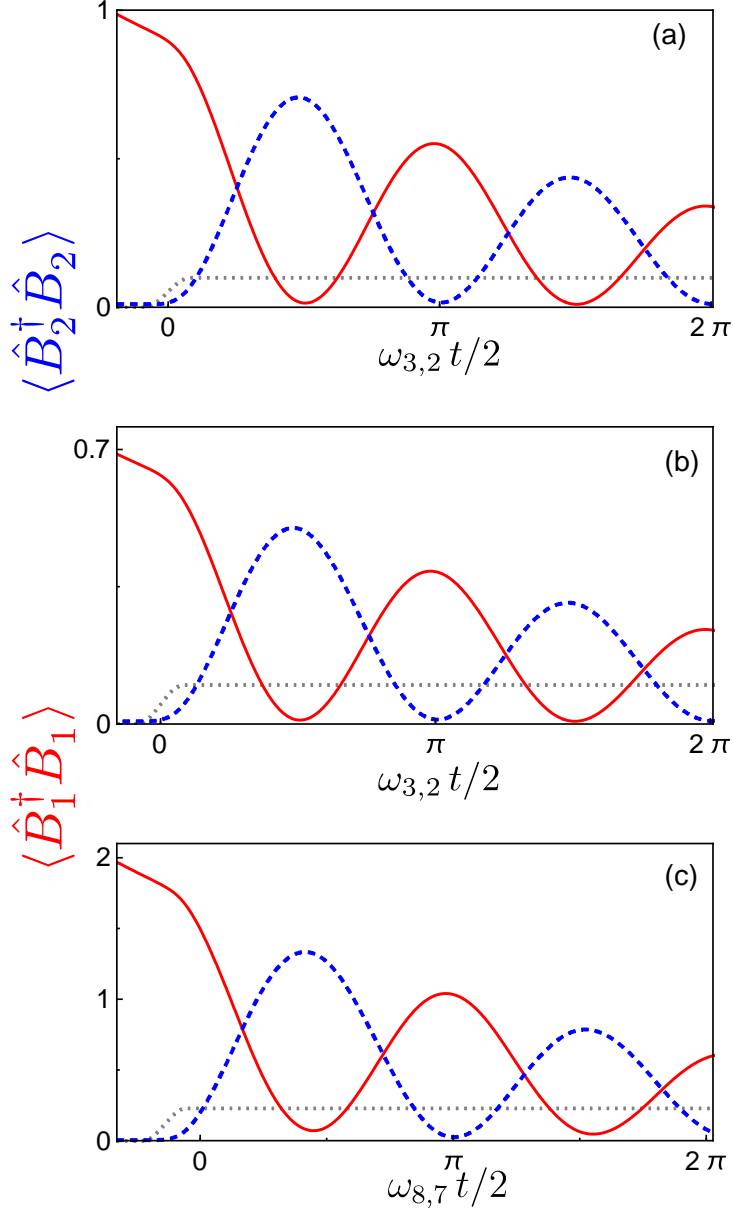
Figure S9. Time evolution of the mean phonon numbers of the two mirrors calculated after a non-adiabatic switching of the interaction, as explained in Fig. S8, but in the presence of losses both in mirrors and cavity. The parameters are the same as in Fig. S8; in addition we have $\gamma = \gamma_1 = \gamma_2 = \omega_1/650$ and $\kappa = 0.5\,\gamma$. The system is initially prepared in the states (a) $|1,0,0\rangle$, (b) $\frac{1}{\sqrt{2}}(|1,0,0\rangle + |0,0,1\rangle)$, (c) $|2,0,0\rangle$. As we can observe, the oscillations are damped and disappear after a few periods. In (c) the losses do not allow for observations of beats oscillations having a longer time period. The dotted gray lines show how the frequency of mirror 2 is tuned into resonance with mirror 1 (details are given in the text).

antisymmetric superpositions of $|1, 0, 0\rangle$ and $|0, 1, 0\rangle$; see Fig. 1b in the main paper). In Fig. S8(c), the avoided level crossing between the states $|\psi_9\rangle$, $|\psi_8\rangle$, and $|\psi_7\rangle$ gives rise to transitions from higher to lower levels. As a consequence, we observe beats between the two transition frequencies $\omega_{8,9}$ and $\omega_{8,7}$ (with the chosen parameters the other frequency transition $\omega_{9,7}$ does not contribute to the beats). Finally, in Fig. S9, we show the time evolution of the mean phonon numbers for the same cases discussed above, but in the presence of losses both in mirrors and cavity. We observe the damping of the population dynamics as expected in presence of losses.

VII. EXPERIMENTAL PLATFORM FOR THE OBSERVATION OF THE PROPOSED EFFECT

A platform to experimentally demonstrate these results is circuit optomechanics using ultra-high-frequency (ω_1 at 4-6 GHz) dilatational resonators [5]. These mechanical oscillators have a resonance frequency $f_m = v/2d$, where v is the average speed of sound and d is the resonator thickness. Their resonant quantum interaction with a superconducting phase qubit, described by the quantum Rabi (or also the Jaynes-Cummings) Hamiltonian, has been experimentally demonstrated [5, 6]. In the present case, we want to estimate the radiation-pressure interaction strength between the high-frequency mechanical resonator and an electromagnetic resonator. In order to estimate the achievable coupling strength, we begin by analyzing the coupling between a mechanical resonator and a flux qubit, experimentally realized in Ref. [5]. Then we use the experimentally achieved qubit-oscillator coupling strength to derive an accurate estimate of the presently achievable radiation-pressure coupling strength between this mechanical resonator and an electromagnetic resonator. Note that the mechanical oscillator considered in Ref. [5] has a quality factor equal to that used in our calculations: $Q = 260$. Moreover, it has been shown that lowering f_m can strongly increase the quality factor [7].

The mechanical resonator is coupled to a superconducting artificial atom through a capacitor [5]. An elastic strain in the vibrational resonator produces, through the piezoelectric effect, a charge on the capacitor enclosing it, which results in a charge Q on the coupling capacitor giving a current $\dot{Q}$. The coupling energy is $\hat{V}' = (\hbar/2e)\,\hat{\varphi}\,\dot{\hat{Q}}$, where $\hat{\varphi}$ is the phase-difference operator of the Josephson junction. Considering only the two lowest energy levels

(qubit) of the artificial atom, the phase operator can be expanded as $\hat{\phi} = (2E'_C/E'_J)^{1/4} \hat{\sigma}_x$, resulting in the Rabi-like interaction Hamiltonian

$$\hat{V}'_{qm} = \hbar \, (2E'_C/E'_J)^{1/4} \, \hat{\sigma}_x \, (\dot{\hat{Q}}/2e) \,, \tag{S37}$$

where E'_C and E'_J are the charging energy and the Josephson energy, respectively, of the phase qubit (with $E'_C \ll E'_J$), and $\dot{\hat{Q}}$ is proportional to the vibrational strain velocity $\dot{\hat{x}} = i\omega_1 X_{\mathrm{zpf}} \, (\hat{b}_1^\dagger - \hat{b}_1)$ (X_{zpf} is the zero-point fluctuation amplitude of the mechanical coordinate). Finally, this interaction Hamiltonian can also be expressed in the standard Rabi interaction form:

$$\hat{V}'_{qm} = -ig'_m(\hat{b} - \hat{b}^\dagger)\hat{\sigma}_x \,, \tag{S38}$$

where g'_m is the resulting coupling strength and $\hat{b}$ and $\hat{b}^\dagger$ are, respectively, the annihilation and creation operators for a generic mechanical oscillator.

For the observation of the effects described in this paper, optomechanical systems displaying a radiation-pressure interaction Hamiltonian are required. Moreover a strong optomechanical coupling (at least $g/\omega_1 \sim 0.01$) is needed. This kind of interaction with a reasonable coupling strength can be obtained by considering a tripartite system consisting of an electromagnetic resonator, an ultra-high-frequency mechanical resonator, and a superconducting charge qubit mediating the interaction between the former two parts [8, 9]. It has been shown that the presence of the qubit can strongly enhance the optomechanical coupling.

Without presenting a detailed circuit-optomechanical setup, which goes beyond the scope of the present work, we can provide an estimate of the resulting coupling strength which can be achieved within state-of-the-art technology. Specifically, considering one generic mechanical oscillator, coupled through a capacitor to a charge qubit, the qubit-mechanical oscillator interaction Hamiltonian can be written as $\hat{V}_{qm} = 8E_C \, \hat{n} \, (\hat{Q}/2e)$, where $\hat{n}$ is the number operator for the Cooper pairs transferred across the junction. In the full charge qubit limit, $E_J \ll E_C$, the bare qubit transition energy is $\omega_q \approx 4E_C$, and the mechanical coupling is longitudinal, i.e., in the two-state representation $\hat{n} \to \hat{\sigma}_z/2$. The resulting interaction Hamiltonian is

$$\hat{V}_{qm} = \hbar\omega_q \, \hat{\sigma}_z(Q/2e) \,, \tag{S39}$$

which can also be expressed as

$$\hat{V}_{qm} = g_m(\hat{b} + \hat{b}^\dagger)\hat{\sigma}_z \,. \tag{S40}$$

Assuming that the same mechanical oscillator is coupled through the same capacitor to the two different kinds of superconducting qubits, it is possible to compare the two qubit-mechanical oscillator coupling strengths. From Eqs (S37) and (S39), disregarding the phase difference, we obtain

$$\frac{g_m}{g_m'} = \left(\frac{E_J'}{2E_C'}\right)^{\frac{1}{4}} \frac{\omega_q}{\omega_1}. \tag{S41}$$

Below we will consider the case $2\omega_q \sim \omega_1$. Assuming the energies E_J' and E_C' for a typical phase qubit (see, e.g. Ref. [7]), we obtain $g_m/g_m' \gtrsim 12$.

Now, following Refs. [8] and [9], we consider the additional interaction of the charge qubit with an electromagnetic resonator, described by the Hamiltonian

$$\hat{V}_{qc} = g_c(\hat{a} + \hat{a}^\dagger)\hat{\sigma}_x, \tag{S42}$$

where $\hat{a}$ is the destruction operator of the cavity mode. In the dispersive regime, the qubit-cavity interaction can be well approximated by [10]

$$\hat{V}_{qc} = (g_c^2/2\Delta)\hat{\sigma}_z(\hat{a} + \hat{a}^\dagger)^2, \tag{S43}$$

where $\Delta = \omega_q - \omega_c$. Corrections of the qubit energy not depending on photon operators have been disregarded. Equation (S40) shows that the coupling of the charge qubit with the mechanical oscillator induces a qubit energy shift depending on the mechanical displacement, so that $\omega_q \to \omega_q + 2g_m(\hat{b} + \hat{b}^\dagger)$. Replacing Δ with $\Delta(\hat{x}) = \omega_q + 2g_m(\hat{b} + \hat{b}^\dagger) - \omega_c$ in Eq. (S43), assuming small displacements, and considering the qubit in its ground state, from Eq. (S43) we obtain the following optomechanical interaction,

$$\hat{H}_I = \frac{g}{2}(\hat{a} + \hat{a}^\dagger)^2(\hat{b} + \hat{b}^\dagger), \tag{S44}$$

with

$$g = \frac{2g_m g_c^2}{\Delta^2}. \tag{S45}$$

Using $g_m = 0.02\,\omega_1$, corresponding to the value of the electromechanical system employed for the demonstration of single-phonon control of a mechanical resonator [5], assuming $g_m/g_m' = 12$, and considering a detuning $\Delta = 5g_c$, we obtain $g \simeq 0.02\omega_1$. The achievable value could be even higher, noting that the electromechanical system used in Ref. [5] was designed to limit g_m in order to optimize the transfer process [7].

Beyond the direct observation of the energy transfer between the mechanical oscillators (see Fig. 1 in the main text), the effective coherent coupling between the two mirrors can also

be demonstrated by looking at the system response (e.g., $\langle \hat{B}_1^\dagger \hat{B}_1 \rangle$) under continuous-wave weak excitation as a function of the excitation frequency. For $\omega_1 = \omega_2$, if $\lambda > \gamma$, two peaks should be observed, corresponding, e.g., to the avoided level crossing at higher energy in Fig. 2(b) in the main text or to that in Fig. S3(a). In order to confirm that the two observed peaks originate from virtual DCE photons, it would be useful to perform measurements changing the optomechanical coupling. This coupling can be tuned by modifying the gate charge of the qubit mediating the interaction [9]. If the energy splitting originates from virtual DCE photons, as predicted by Eq. (3) in the main text, it should grow quadratically with the optomechanical coupling g (see Fig. S1). The anticrossing behaviour could also be probed, changing d of one of the two dilatational resonators and detecting, e.g., $\langle \hat{B}_1^\dagger \hat{B}_1 \rangle$ at steady state as a function of the thickness d (note that $\omega_2 = v/d$). Two peaks with a splitting determined by the thickness, following the avoided level crossing should be observed (see, e.g., Fig. S3). The detection of the mechanical excitations can be performed following the procedures used in Refs. [7, 11].

[1] C. K. Law, "Interaction between a moving mirror and radiation pressure: A Hamiltonian formulation," Phys. Rev. A **51**, 2537 (1995).

[2] V. Macrì, A. Ridolfo, O. Di Stefano, A. F. Kockum, F. Nori, and S. Savasta, "Nonperturbative dynamical casimir effect in optomechanical systems: Vacuum casimir-rabi splittings," Phys. Rev. X **8**, 011031 (2018).

[3] M. O. Scully and M. S. Zubairy, *Quantum Optics* (Cambridge University Press, 1997).

[4] W. Shao, C. Wu, and X.-L. Feng, "Generalized James' effective Hamiltonian method," Phys. Rev. A **95**, 032124 (2017).

[5] A. D. O'Connell, M. Hofheinz, M. Ansmann, R. C. Bialczak, M. Lenander, E. Lucero, M. Neeley, D. Sank, H. Wang, M. Weides, *et al.*, "Quantum ground state and single-phonon control of a mechanical resonator," Nature **464**, 697 (2010).

[6] F. Rouxinol, Y. Hao, F. Brito, A. O. Caldeira, E. K. Irish, and M. D. LaHaye, "Measurements of nanoresonator-qubit interactions in a hybrid quantum electromechanical system," Nanotechnology **27**, 364003 (2016).

[7] A. N. Cleland and M. R. Geller, "Superconducting qubit storage and entanglement with

nanomechanical resonators," Phys. Rev. Lett. **93**, 070501 (2004).

[8] T. T. Heikkilä, F. Massel, J. Tuorila, R. Khan, and M. A. Sillanpää, "Enhancing optome-chanical coupling via the Josephson effect," Phys. Rev. Lett. **112**, 203603 (2014).

[9] J.-M. Pirkkalainen, S. U. Cho, F. Massel, J. Tuorila, T. T. Heikkilä, P. J. Hakonen, and M. A. Sillanpää, "Cavity optomechanics mediated by a quantum two-level system," Nat. Commun. **6**, 6981 (2015).

[10] D. Zueco, G. M. Reuther, S. Kohler, and P. Hänggi, "Qubit-oscillator dynamics in the disper-sive regime: Analytical theory beyond the rotating-wave approximation," Phys. Rev. A **80**, 033846 (2009).

[11] A. O'Connell and A. N. Cleland, "Microwave-frequency mechanical resonators operated in the quantum limit," in *Cavity Optomechanics* (Springer, 2014) pp. 253–281.